Elasticity equations with random domains—the shape derivative approach

M. Clarke[1] J. Dick[2] Q. T. Le Gia[3] D. Pye[4]

(Received 31 December 2020; revised 17 February 2022)

Abstract

In this work, we discuss elasticity equations on a two-dimensional domain with random boundaries and we apply these equations to modelling human corneas.

Contents

DOI:10.21914/anziamj.v62.16120, Published 2022-03-09, as part of the Proceedings of the 19th Biennial Computational Techniques and Applications Conference. ISSN 1445-8810.

1 Introduction

In this article we analyse how the solution of the linear elasticity equation behaves as a function of (stochastic) perturbations of the domain. This is a recent research area of uncertainty quantification in which we assign random fields to parameters in a partial differential equation (PDE) model. In general, the output goal is to compute some functionals of the solution which yield useful statistics such as expectation, variance or correlation.

There are many potential applications of this problem, such as shape optimisation of airfoils, sensitivity analysis in structural design, tomography in medical imaging and seismology [14], minimal surfaces, and biological membranes and molecular structures [4, 2]. As a concrete application of the method, we construct a simple elasticity model of human corneas from different individuals.

The novel features of the article are listed as follows. Firstly, while the numerical analysis in shape derivatives for elliptic PDEs with a stochastic boundary [12, 10, 11] is widely available, a similar analysis for elasticity equations does not exist in the literature. Secondly, we propose a new way to approximate the expectation of the random solution of the random boundary problem using a higher order quasi-Monte Carlo method [6], which has not been carried out before even for elliptic random boundary problems. The higher order quasi-Monte Carlo rules employed in this article are based on interlaced polynomial lattice point rules [9] and we compare this method with a randomized quasi-Monte Carlo method based on scrambled interlaced Sobol points [5].

2 Linear elasticity with random domains

Let $D \subset \mathbb{R}^2$ be a bounded, closed and connected domain with boundary $\partial D \in C^{k+1}$ for $k > 3$. Let $\mathbf{f}$ be the body force within D and $\mathbf{g}$ be the traction force tangential to ∂D. The linear elasticity equation on D reads

$$-\nabla \cdot \boldsymbol{\sigma} = \mathbf{f} \quad \text{in } D\,, \tag{1}$$

$$\mathbf{u} = \mathbf{g} \quad \text{in } \partial D\,. \tag{2}$$

Here $\mathbf{u}$ is the displacement vector, and $\boldsymbol{\sigma}$ is the Cauchy stress tensor which relates to the resistance of internal forces exerted by neighbouring particles over some surface element. By Hooke's law we have

$$\boldsymbol{\sigma} = \mathcal{C}\boldsymbol{\varepsilon}(\mathbf{u}) = \lambda(\operatorname{tr}\boldsymbol{\varepsilon})I + 2\mu\boldsymbol{\varepsilon}\,, \tag{3}$$

where λ and μ are the Lamé parameters, $\mathcal{C}$ is Hooke's tensor, and the strain tensor is

$$\boldsymbol{\varepsilon}(\mathbf{u}) = \tfrac{1}{2}\left[\nabla\mathbf{u} + (\nabla\mathbf{u})^T\right], \tag{4}$$

which relates to the change in displacement relative to a reference configuration for small $\mathbf{u}$ and $\nabla\mathbf{u}$.

Now suppose the boundary ∂D is perturbed randomly in an $O(\delta)$ layer which yields a family of boundaries ∂D_δ, where we assume that $\delta > 0$ is sufficiently small. As κ varies, the curve ∂D_δ is perturbed from the fixed curve ∂D with the perturbation $\delta\kappa(\mathbf{x},\omega)\mathbf{n}$. Let $(\Omega, \Sigma, \mathbb{P})$ be a suitable probability space. We parameterize the deformed boundary ∂D_δ using a random field $\kappa(\cdot,\cdot) : \partial D \times \Omega \to \mathbb{R}$ for samples $\omega \in \Omega$,

$$\partial D_\delta = \{\mathbf{x} + \delta\kappa(\mathbf{x},\omega)\mathbf{n} : \mathbf{x} \in \partial D\}, \tag{5}$$

where $\mathbf{n}$ is the exterior unit normal vector to the reference boundary ∂D.

Similar to Harbrecht [12, Eq. (3.3)] we assume that

$$\|\kappa(\cdot,\omega)\|_{C^k(\partial D)} \leqslant 1$$

for $\mathbb{P}$ almost all $\omega \in \Omega$.

Assume that the random field κ admits the Karhunen–Loéve expansion [15]

$$\kappa(x, \omega) = \kappa_0 + C \sum_{j=1}^{\infty} K_j(\omega) \sqrt{\gamma_j} \psi_j(x) . \tag{6}$$

We use random variables $K_j(\omega) \sim U(-1, 1)$ where $U(a, b)$ denotes the uniform distribution over (a, b), $\kappa_0 = 0$ and the constant $C > 0$ is such that $\operatorname{ess\,sup}_{x \in D, \omega \in \Omega} |\kappa(x, \omega)| = 1$ and expectation

$$\mathbb{E}[\kappa(x, \cdot)] = 0 . \tag{7}$$

We interpret the deformation of the boundary using the flow of a vector field [4, Chapter 8],[13]. Let $V : D \to M \subset \mathbb{R}^2$ be a Lipschitz continuous vector field on a two-dimensional manifold M. For $\mathbf{x} \in M$ the velocity vectors in V induce a flow $\phi(t, \mathbf{x})$ and are tangential to the integral curves of the vector field yielded from the ODE

$$\frac{\partial \phi(t, \mathbf{x})}{\partial t} = V(\mathbf{x}) , \quad \phi(0, \mathbf{x}) = \mathbf{x} , \quad \text{for all } \mathbf{x} \in D .$$

The perturbation field $V_\delta : D \times \Omega \to M \subset \mathbb{R}^2$ deforms the boundary ∂D with the velocity at $t = 0$ of the flow field $V_\delta(\mathbf{x}, \omega) = \delta\kappa(\mathbf{x}, \omega)\mathbf{n}$. We think of the boundary perturbation as a diffeomorphism

$$\partial D \mapsto \partial D_\delta = [I + V(\omega)]\mathbf{x} = \{\phi(\delta, \mathbf{x}, \omega) : \mathbf{x} \in \partial D\} ,$$

where I is the identity operator.

We consider the boundary value problem that models the elasticity of the domain with the perturbed boundary

$$-\nabla \cdot \boldsymbol{\sigma}_\delta = \mathbf{f} \quad \text{in } D_\delta , \quad \boldsymbol{\sigma}_\delta = \mathcal{C}\boldsymbol{\varepsilon}(\mathbf{u}_\delta) , \quad \mathbf{u}_\delta = \mathbf{g} \quad \text{on } \partial D_\delta ,$$

where as before $\mathcal{C}$ is Hooke's tensor and $\boldsymbol{\sigma}_\delta$ is the Cauchy's stress tensor.

Let us define the transportation of a vector $\mathbf{u}_\delta$ along the flow for $t \in [0, \delta]$ by

$$\mathbf{u}^t(\mathbf{x}, \omega) = \mathbf{u}_\delta(\phi(t, \mathbf{x}, \omega), \omega)\,, \quad \mathbf{u}^0(\mathbf{x}, \omega) = \mathbf{u}_\delta(\phi(0, \mathbf{x}, \omega), \omega)\,.$$

The Lagrangian or 'material' derivative for $\mathbf{x} \in D \cap D_\delta$ is defined by

$$\dot{\mathbf{u}}(\mathbf{x}, \omega) = \lim_{t \to 0^+} \frac{\mathbf{u}^t(\phi(t, \mathbf{x}, \omega), \omega) - \mathbf{u}^0(\mathbf{x}, \omega)}{t}\,, \quad 0 < t \leqslant \delta\,.$$

Taking the total derivative at pseudo-time $t = 0$, we obtain

$$\begin{aligned} \dot{\mathbf{u}}(\mathbf{x}, \omega) &= \left.\frac{\partial \mathbf{u}^0(\phi(t, \mathbf{x}, \omega), \omega)}{\partial t}\right|_{t=0} + \nabla \mathbf{u}^0(\mathbf{x}, \omega) \cdot \left.\frac{\partial \phi(t, \mathbf{x}, \omega)}{\partial t}\right|_{t=0} \\ &= d\mathbf{u}(\mathbf{x}, \omega) + \nabla \mathbf{u}_\delta \cdot V_\delta(\mathbf{x}, \omega)\,, \end{aligned} \tag{8}$$

where the Eulerian or local shape derivative $d\mathbf{u}$ is defined pointwise by

$$d\mathbf{u}(\mathbf{x}) = \lim_{\delta \to 0^+} \frac{\mathbf{u}_\delta(\mathbf{x}) - \mathbf{u}^0(\mathbf{x})}{\delta}\,, \quad \mathbf{x} \in D \cap D_\delta\,.$$

3 Weak formulation

Without loss of generality (or by introducing a new variable [3]), we assume $\mathbf{g} = \mathbf{0}$ in (2). The weak formulation of (1) under the zero Dirichlet condition is to find the solution of the unperturbed problem $\bar{\mathbf{u}} \in H^2(D) \cap H_0^1(D)$ so that

$$-\int_D [\nabla \cdot \boldsymbol{\sigma}(\bar{\mathbf{u}})] \cdot \boldsymbol{\nu}\, d\mathbf{x} = \int_D \mathbf{f} \cdot \boldsymbol{\nu}\, d\mathbf{x}\,, \quad \text{for all } \boldsymbol{\nu} \in H_0^1(D)\,. \tag{9}$$

Using integration by parts, equation (9) is written as

$$2\mu \int_D \boldsymbol{\varepsilon}(\bar{\mathbf{u}}) : \boldsymbol{\varepsilon}(\boldsymbol{\nu})\, d\mathbf{x} + \lambda \int_D (\nabla \cdot \bar{\mathbf{u}})(\nabla \cdot \boldsymbol{\nu})\, d\mathbf{x} = \int_D \mathbf{f} \cdot \boldsymbol{\nu}\, d\mathbf{x}\,, \tag{10}$$

where for two general tensors $\boldsymbol{\varepsilon}$ and $\bar{\boldsymbol{\varepsilon}}$, we set $\boldsymbol{\varepsilon} : \bar{\boldsymbol{\varepsilon}} = \sum_i \sum_j \varepsilon_{i,j} \bar{\varepsilon}_{i,j}$.

Let us define the bilinear form

$$a(\bar{\mathbf{u}}, \boldsymbol{v}) := 2\mu \int_D \boldsymbol{\varepsilon}(\bar{\mathbf{u}})\colon \boldsymbol{\varepsilon}(\boldsymbol{v})\, d\mathbf{x} + \lambda \int_D (\nabla \cdot \bar{\mathbf{u}})(\nabla \cdot \boldsymbol{v})\, d\mathbf{x}$$

and the linear functional

$$\ell_1(\boldsymbol{v}) = \int_D \mathbf{f} \cdot \boldsymbol{v}\, d\mathbf{x}\,, \quad \boldsymbol{v} \in H_0^1(D)\,.$$

We then write (10) as

$$a(\bar{\mathbf{u}}, \boldsymbol{v}) = \ell_1(\boldsymbol{v})\,, \quad \text{for all } \boldsymbol{v} \in H_0^1(D)\,. \tag{11}$$

The weak formulation for equation (10) on D_δ is to find $\mathbf{u}_\delta \in H^1(D_\delta)$ so that

$$a_\delta(\mathbf{u}_\delta, \boldsymbol{v}) = \ell_2(\boldsymbol{v})\,, \quad \text{for all } \boldsymbol{v} \in H^1(D_\delta)\,, \tag{12}$$

where

$$a_\delta(\mathbf{u}_\delta, \boldsymbol{v}) = 2\mu \int_{D_\delta} \boldsymbol{\varepsilon}(\mathbf{u}_\delta)\colon \boldsymbol{\varepsilon}(\boldsymbol{v})\, d\mathbf{x} + \lambda \int_{D_\delta} (\nabla \cdot \mathbf{u}_\delta)(\nabla \cdot \boldsymbol{v})\, d\mathbf{x}$$

and

$$\ell_2(\boldsymbol{v}) = \int_{D_\delta} \mathbf{f} \cdot \boldsymbol{v}\, d\mathbf{x}\,.$$

To understand the relation between $\bar{\mathbf{u}}$ and $\mathbf{u}_\delta$ we consider Taylor's expansion of the solution $\mathbf{u} = \mathbf{u}(\phi(t, \mathbf{x}, \omega), \omega)$ at pseudo-time $\delta = 0$ under the action of the flow $\phi(t, \mathbf{x})$ for $t \in [0, \delta]$ where the derivatives are defined in the Lagrangian sense. For $\mathbf{u}_\delta(\mathbf{x}, \omega) = \mathbf{u}(\phi(\delta, \mathbf{x}, \omega), \omega)$ we have

$$\mathbf{u}_\delta(\mathbf{x}, \omega) = \bar{\mathbf{u}}(\mathbf{x}) + \delta d\mathbf{u}(\mathbf{x}, \omega) + O(\delta^2)\,, \quad \mathbf{x} \in K \subset \bigcap_{\omega \in \Omega} D(\omega)\,. \tag{13}$$

In the following theorem we consider the expectation and covariance of the random solutions [12, Section 4.2].

Theorem 1. *With the assumptions above, the expectation and covariance of the random solution of the elasticity equation with random boundary* D_δ *satisfy*

$$\mathbb{E}[\mathbf{u}_\delta] = \bar{\mathbf{u}} + O(\delta^2) \quad \textit{in } K\,, \tag{14}$$
$$\operatorname{Cov}[\mathbf{u}_\delta] = \delta^2 \mathbb{E}[\mathbf{du} \otimes \mathbf{du}] + O(\delta^3) \quad \textit{in } K \times K\,, \tag{15}$$

where $\bar{\mathbf{u}} \in H^1(D)$ *solves the deterministic problem on the nominal domain* D*.*

Proof: We outline the main ideas [12, Section 4.2 for more details]. Using the assumption (7) and the properties of $\mathbf{du}$, we have

$$\mathbb{E}[\mathbf{du}(\mathbf{x},\omega)] = -\mathbb{E}[\kappa(\mathbf{x},\cdot)]\frac{\partial \bar{\mathbf{u}}}{\partial \mathbf{n}} = 0 \quad \text{on } \partial D\,.$$

Thus the first order term in the shape Taylor expansion (13) vanishes. Hence (14) follows. Equation (15) follows from the properties of the variance,

$$\operatorname{Cov}[\mathbf{u}_\delta] = \mathbb{E}[\mathbf{u}_\delta]^2 - (\mathbb{E}[\mathbf{u}_\delta])^2\,.$$

From the Taylor expansion

$$\mathbf{u}_\delta(\mathbf{x},\omega) = \bar{\mathbf{u}}(\mathbf{x}) + \delta \mathbf{du}(\mathbf{x},\omega) + \tfrac{\delta^2}{2} d^2\mathbf{u}(\mathbf{x},\omega) + O(\delta^3)$$

we have

$$\begin{aligned}
\mathbb{E}[(\mathbf{u}_\delta(\mathbf{x},\omega)^2] &= \mathbb{E}\left[[\bar{\mathbf{u}}(\mathbf{x}) + \delta \mathbf{du}(\mathbf{x},\omega) + \tfrac{\delta^2}{2} d^2\mathbf{u}(\mathbf{x},\omega) + O(\delta^3)]^2\right] \\
&= \bar{\mathbf{u}}^2(\mathbf{x}) + \delta^2 \mathbb{E}[\mathbf{du}^2(\mathbf{x},\omega)] + 2\delta\bar{\mathbf{u}}\mathbb{E}[\mathbf{du}(\mathbf{x},\omega)] \\
&\quad + \delta^2 \bar{\mathbf{u}}(\mathbf{x})\mathbb{E}[d^2\mathbf{u}(\mathbf{x},\omega)] + O(\delta^3)\,.
\end{aligned} \tag{16}$$

On the other hand

$$\begin{aligned}
(\mathbb{E}[\mathbf{u}_\delta(\mathbf{x},\omega]])^2 &= \Big(\mathbb{E}[\bar{\mathbf{u}}(\mathbf{x}) + \delta \mathbf{du}(\mathbf{x},\omega) + \tfrac{\delta^2}{2} d^2\mathbf{u}(\mathbf{x},\omega) + O(\delta^3)]\Big)^2 \\
&= \Big(\bar{\mathbf{u}}(\mathbf{x}) + \delta\mathbb{E}[\mathbf{du}(\mathbf{x},\omega)] + \tfrac{\delta^2}{2}\mathbb{E}[d^2\mathbf{u}(\mathbf{x},\omega)] + O(\delta^3)\Big)^2
\end{aligned}$$

$$= \bar{u}^2(x) + \delta^2\mathbb{E}^2[du(x,\omega)] + 2\delta\bar{u}\mathbb{E}[du(x,\omega)] + \delta^2\bar{u}(x)\mathbb{E}[d^2u(x,\omega)] + O(\delta^3)\,. \tag{17}$$

Subtracting equations (16) and (17) we obtain the desired result. ♠

To construct an approximate solution using a finite element method, we denote by W_h the space of vectors that each component is a piece-wise linear function. The Galerkin approximation problem for (11) is: find $\mathbf{u}_h \in W_h$ so that

$$a(\mathbf{u}_h, \mathbf{v}) = \ell_1(\mathbf{v})\,, \quad \text{for all } \mathbf{v} \in W_h\,. \tag{18}$$

We approximate $\mathbb{E}\mathbf{u}_\delta$ using a higher order quasi-Monte Carlo method [6] by discretising the sample space of κ defined in (6) with

$$\kappa(\mathbf{x}, \mathbf{y}) = \kappa_0 + C\sum_{j=1}^{s} y_j\psi_j(\mathbf{x})\,,$$

where $\mathbf{y} = (y_1, y_2, \ldots, y_s) \in \mathbb{R}^s$ is a point in a set of N quasi-Monte Carlo quadrature points $\{\mathbf{y}^{(1)}, \mathbf{y}^{(2)}, \ldots, \mathbf{y}^{(N)}\}$ for some given truncated dimension s. Then

$$\mathbb{E}[\mathbf{u}_\delta(\mathbf{x})] \approx \frac{1}{N}\sum_{k=1}^{N} \mathbf{u}_\delta(\mathbf{x}, \mathbf{y}^{(k)})\,.$$

The approximation error of quasi-Monte Carlo quadrature of N quadrature points is of order $O(N^{-\lambda})$ with $\lambda \geqslant 2$ [6].

4 Numerical experiments

The numerical experiments presented in this section are inspired by an application in optometry and vision science. We model the elasticity of human corneas of different individuals using the elasticity equation on random domains. This is motivated by the random parameters of the human corneas [1, 7, 8, 18, 19, 16] listed in Table 1.

Table 1: parameters of the human cornea.

Anterior corneal curvature	Mean radius $= 7.74 \pm 0.26\,\mathrm{mm}$
Posterior corneal curvature	Mean radius $= 7.18 \pm 0.28\,\mathrm{mm}$
Central corneal thickness	$545.94 \pm 36.76\,\mu\mathrm{m}$
Peripheral corneal thickness	$821 \pm 56\,\mu\mathrm{m}$
Corneal diameter	Horizontal $= 11.81 \pm 0.65\,\mathrm{mm}$
	Vertical $= 11.26 \pm 0.64\,\mathrm{mm}$
Intraocular pressure	$15.06 \pm 2.71\,\mathrm{mmHg}$
Young's modulus of the cornea	$0.29 \pm 0.06\,\mathrm{MPa}$

Figure 1 captures the parameters in Table 1 in a simple geometry sketch, where the mean radius of the anterior cornea is denoted by $b + d_c$, the mean radius of the posterior is denoted b, central corneal thickness is denoted by d_c, and the peripheral thickness is denoted d_p. From the diagram, we extract the approximation of the human cornea, given in Figure 2. The random boundary is modelled by (5) with $x = (a\cos\theta, b\sin\theta)$ (for the inner ellipse) or $x = ((a + d_a)\cos\theta, (b + d_c)\sin\theta)$ (for the outer ellipse) and

$$\kappa(\theta, y) = \sum_{j=1}^{5} y_j \cos(j\theta) + y_j \sin(j\theta)\,,$$

where $y = (y_1, \dots, y_5)$ is selected from a set of $N = 1\,024$ higher order quasi-Monte Carlo points. We then use Matlab's PDE analysis model

```
createpde('structural','static-planestress')
```

to solve the elastic equation for the fixed cornea and for each realisation of the randomised corneas.

The Young's modulus is $0.25 \times 10^6\,\mathrm{Pa}$, the Poisson's ratio is 0.49 and the pressure on the posterior (inner) curve is set to $2.0078 \times 10^3\,\mathrm{Pa}$. For the fixed cornea, $88\,371$ quadratic finite elements over a triangular mesh with $178\,300$ nodes with mesh size $\tau = 0.01$ is used to compute the reference

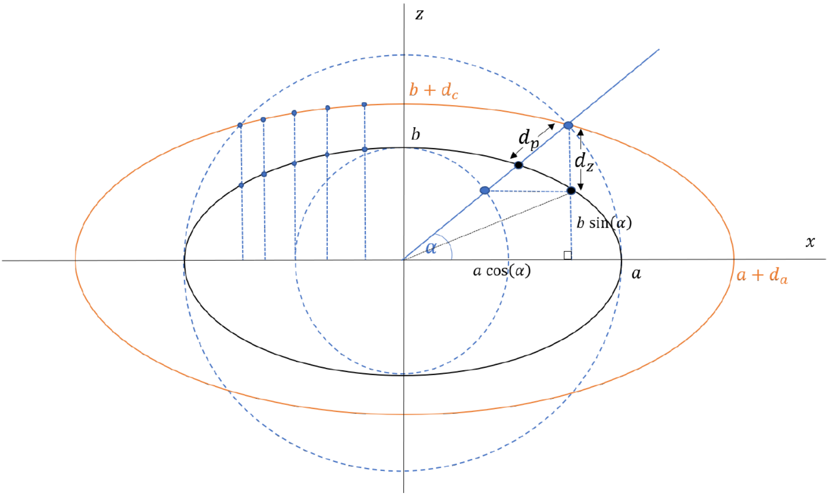

Figure 1: a diagram which captures the parameters in Table 1 to construct the domains which model human corneas.

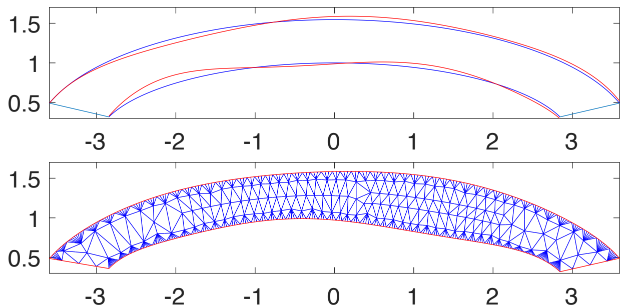

Figure 2: (left) the domain with a random boundary; and (right) its finite element mesh.

Table 2: The numerical errors between the numerical solutions $\bar{\mathbf{u}}_h$ on the fixed domain D and reference solution $\bar{\mathbf{u}}_*$ with different mesh sizes h. Here E is the number of quadratic finite elements and M is the number of nodes in the mesh.

h	$\lVert e_x \rVert$	$\lVert e_y \rVert$	$\lVert e_x \rVert_\infty$	$\lVert e_y \rVert_\infty$	E	M
0.500	2.60×10^{-4}	7.51×10^{-4}	6.90×10^{-4}	1.49×10^{-3}	468	1341
0.250	1.58×10^{-4}	3.73×10^{-4}	3.97×10^{-4}	1.30×10^{-3}	710	1827
0.125	8.01×10^{-5}	1.47×10^{-4}	2.94×10^{-4}	9.72×10^{-4}	1304	3021
0.0625	2.86×10^{-5}	4.80×10^{-5}	1.64×10^{-4}	5.42×10^{-4}	2852	6129

solution $\bar{\mathbf{u}}_*$. The ℓ_2 and ℓ_∞ errors between $\bar{\mathbf{u}}_*$ and $\bar{\mathbf{u}}_h$ for different mesh sizes are given in Table 2. For the randomised cornea, the number of quadratic finite elements ranges from $2\,732$ to $2\,948$ defined on triangular meshes (with mesh size $h = 0.0625$) with the number of nodes ranging from $5\,889$ to $6\,321$. A realisation of the triangular mesh is shown in the right panel of Figure 2. In the current implementation, generating each mesh took less than 0.8 s on a MacBook pro 2.6 GHz with 16 G of RAM. However, for a more challenging domain, mesh generation time could be saved if only the part of the domain close to the random boundary is re-meshed for each new realisation.

We approximate $\mathbb{E}[\mathbf{u}_{h,\delta}]$ using the higher order quasi-Monte Carlo method by

$$\mathbb{E}[\mathbf{u}_{h,\delta}] \approx Q_N(\mathbf{u}_{h,\delta}) = \frac{1}{N} \sum_{k=1}^{N} \mathbf{u}_{h,\delta}(\boldsymbol{x}, \boldsymbol{y}^{(k)}).$$

We note that $\mathbf{u}_{h,\delta}$ is a vector in $\mathbb{R}^2$, that is, $\mathbf{u}_{h,\delta} = (u^x_{h,\delta}, u^y_{h,\delta})$. The ℓ_2 and ℓ_∞ component errors between $\mathbb{E}[\mathbf{u}_{h,\delta}]$ and $\bar{\mathbf{u}}_* = (\bar{u}^x_*, \bar{u}^y_*)$ are defined by

$$\lVert e_x \rVert := \left(\frac{1}{|\mathcal{G}|} \sum_{\boldsymbol{z} \in \mathcal{G}} |Q_N(u^x_{h,\delta}(\boldsymbol{z})) - \bar{u}^x_*(\boldsymbol{z})|^2 \right)^{1/2},$$

$$\lVert e_y \rVert := \left(\frac{1}{|\mathcal{G}|} \sum_{\boldsymbol{z} \in \mathcal{G}} |Q_N(u^y_{h,\delta}(\boldsymbol{z})) - \bar{u}^y_*(\boldsymbol{z})|^2 \right)^{1/2},$$

Table 3: Numerical errors between $Q_N(\mathbf{u}_{h,\delta})$ and $\bar{\mathbf{u}}_*$ with different values of δ using $N = 2^{10}$ interlaced polynomial lattice points.

δ	$\|e_x\|$	$\|e_y\|$	$\|e_x\|_\infty$	$\|e_y\|_\infty$
0.1000	4.99×10^{-3}	1.03×10^{-2}	2.58×10^{-2}	1.37×10^{-1}
0.0500	3.23×10^{-3}	1.63×10^{-2}	9.56×10^{-3}	4.00×10^{-2}
0.0250	1.01×10^{-3}	5.26×10^{-3}	2.70×10^{-3}	1.02×10^{-2}
0.0125	2.66×10^{-4}	1.44×10^{-3}	7.03×10^{-4}	2.56×10^{-3}

$$\|e_x\|_\infty := \max_{z\in\mathcal{G}} |Q_N(u^x_{h,\delta}(\boldsymbol{z})) - \bar{u}^x_*(\boldsymbol{z})|\,,$$
$$\|e_y\|_\infty := \max_{z\in\mathcal{G}} |Q_N(u^y_{h,\delta}(\boldsymbol{z})) - \bar{u}^y_*(\boldsymbol{z})|\,,$$

where $\mathcal{G}$ is the set of $178\,300$ nodes of a finite element mesh. Theorem 1 shows the dependence of the solution on δ. In our numerical experiments we see a similar behaviour of the numerical solution for different values of δ, that is the numerical errors (for $\delta < 0.1$) are of order $O(\delta^2)$ as shown in Tables 3 and 4. An analogous result of Theorem 1 for the numerical approximation requires a full error analysis of the approximation method, which is left for future work.

The von Mises stress [17] and displacement magnitudes of the solution to the elastic equation for one realisation are given in Figures 3 and 4, respectively.

In this example, quadrature points are obtained from interlacing higher order polynomial lattice point sets [6]. In Table 4 we use the same example, but use scrambled, interlaced Sobol points [5]. In this method, the estimator is a random variable which has the advantage that one can obtain a statistical error estimate via an unbiased estimator of the standard deviation, given by

$$\sqrt{\frac{1}{q-1}\sum_{\nu=1}^{q}[Q_N^{(\nu)}(\mathbf{u}_{h,\delta}) - \overline{Q}_N(\mathbf{u}_{h,\delta})]^2}\,,$$

where $Q_N^{(\nu)}(\mathbf{u}_{h,\delta})$, $\nu = 1,2,\ldots,q$, are q independent estimations of the expectation value and $\overline{Q}_N(\mathbf{u}_{h,\delta}) = q^{-1}\sum_{\nu=1}^{q} Q_N^{(\nu)}(\mathbf{u}_{h,\delta})$ is an estimation of the mean.

Table 4: Numerical errors between $Q_N(u_{h,\delta})$ and $\bar{u}_*$ with different values of δ using $N = 2^{10}$ scrambled, interlaced Sobol points (upper half of table) and estimations of the standard deviations (lower half of table) using $q = 16$ estimations.

δ	$\|e_x\|$	$\|e_y\|$	$\|e_x\|_\infty$	$\|e_y\|_\infty$
0.1000	3.25×10^{-3}	5.18×10^{-3}	2.34×10^{-2}	6.68×10^{-2}
0.0500	2.83×10^{-3}	1.46×10^{-2}	8.73×10^{-3}	3.93×10^{-2}
0.0250	8.68×10^{-4}	4.71×10^{-3}	2.45×10^{-3}	9.59×10^{-3}
0.0125	1.92×10^{-4}	9.97×10^{-4}	5.77×10^{-4}	2.00×10^{-3}
δ	std. $\|e_x\|$	std. $\|e_y\|$	std. $\|e_x\|_\infty$	std. $\|e_y\|_\infty$
0.1000	2.41×10^{-4}	6.18×10^{-4}	1.02×10^{-3}	6.01×10^{-3}
0.0500	3.34×10^{-5}	2.30×10^{-4}	9.91×10^{-5}	2.87×10^{-5}
0.0250	4.34×10^{-6}	1.87×10^{-5}	1.86×10^{-5}	3.74×10^{-6}
0.0125	6.22×10^{-7}	2.41×10^{-6}	4.39×10^{-6}	2.89×10^{-6}

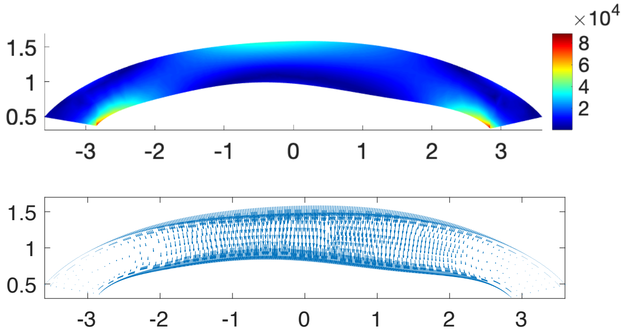

Figure 3: (left) von Mises stress; and (right) vector displacement quiver plot.

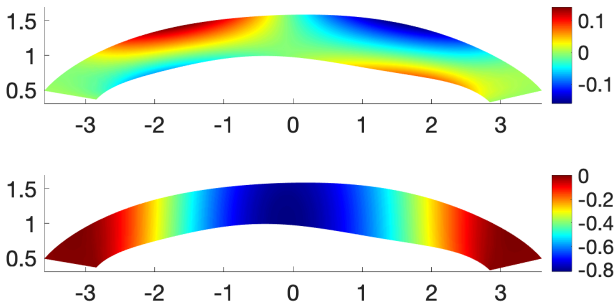

Figure 4: displacement magnitudes (in mm) in (left) x and (right) y directions.

5 Conclusions

We have discussed a numerical method to solve two-dimensional linear elasticity with a random Dirichlet boundary condition and applied the techniques to modelling human corneas with different shapes and sizes. The topic will be of interests to mathematicians and medical scientists of interdisciplinary research.

Acknowledgements The authors gratefully acknowledge the support of the Australian Research Council, in particular, J.D. was supported by DP190101197 and Q.L.G. was supported by DP180100506. Helpful suggestions from the anonymous referees are also gratefully acknowledged.

References

[1] R. C. Augustyn, D. Nankivil, A. Mohamed, B. Maceo, F. Pierre, and J.-M. Parel. "Human ocular biometry". In: *Exp. Eye Res.* 102 (2012), pp. 70–75. DOI: 10.1016/j.exer.2012.06.009. (Cit. on p. C263).

[2] F. Ballarin, A. Manzoni, G. Rozza, and S. Salsa. “Shape optimization by free-form deformation: Existence results and numerical solution for Stokes flows”. In: *J. Sci. Comput.* 60.3 (2014), pp. 537–563. DOI: 10.1007/s10915-013-9807-8. (Cit. on p. C257).

[3] S. C. Brenner and L.-Y. Sung. “Linear finite element methods for planar linear elasticity”. In: *Math. Comp.* 59 (1992), pp. 321–338. DOI: 10.2307/2153060. (Cit. on p. C260).

[4] M. C. Delfour and J.-P. Zolesio. *Shapes and geometries*. Advances in Design and Control. SIAM, Philadelphia, 2001. DOI: 10.1137/1.9780898719826. (Cit. on pp. C257, C259).

[5] J. Dick. “Higher order scrambled digital nets achieve the optimal rate of the root mean square error for smooth integrands”. In: *Ann. Statist.* 39.3 (2011), pp. 1372–1398. DOI: 10.1214/11-AOS880. (Cit. on pp. C257, C267).

[6] J. Dick, F. Y. Kuo, Q. T. Le Gia, and Ch. Schwab. “Multilevel higher order QMC Petrov–Galerkin discretization for affine parametric operator equations”. In: *SIAM J. Num. Anal.* 4.54 (2015), pp. 2541–2568. DOI: 10.1137/16M1078690 (cit. on pp. C257, C263, C267).

[7] A. Eilaghi, J. G. Flanagan, I. Tertinegg, C. A. Simmons, G. W. Brodland, and C. R. Ethier. “Biaxial testing of human sclera”. In: *J. Biomech.* 43 (2010), pp. 1696–1701. DOI: 10.1016/j.jbiomech.2010.02.031. (Cit. on p. C263).

[8] U. Fares, A. M Otri, M. A. Al-Aqaba, and H. S. Dua. “Correlation of central and peripheral corneal thickness in healthy corneas.” In: *Cont. Lens Anterior Eye* 35 (2012), pp. 39–45. DOI: 10.1016/j.clae.2011.07.004. (Cit. on p. C263).

[9] R. N. Gantner and Ch. Schwab. “Computational higher order quasi-Monte Carlo integration”. In: *Monte Carlo and quasi-Monte Carlo methods*. Vol. 163. Springer Proc. Math. Stat. Springer, 2016,

pp. 271–288. DOI: 10.1007/978-3-319-33507-0_12. (Cit. on p. C257).

[10] H. Harbrecht. “Second moment analysis for Robin boundary value problems on random domains”. In: *Singular Phenomena and Scaling in Mathematical Models*. Ed. by M. Griebel. Springer, 2014, pp. 361–381. DOI: 10.1007/978-3-319-00786-1_16. (Cit. on p. C257).

[11] H. Harbrecht, M. Peters, and M. Siebenmorgen. “Analysis of the domain mapping method for elliptic diffusion problems on random domains”. In: *Numer. Math.* 134.4 (2016), pp. 823–856. DOI: 10.1007/s00211-016-0791-4. (Cit. on p. C257).

[12] H. Harbrecht, R. Schneider, and Ch. Schwab. “Sparse second moment analysis for elliptic problems in stochastic domains”. In: *Numer. Math.* 109.3 (2008), pp. 385–414. DOI: 10.1007/s00211-008-0147-9. (Cit. on pp. C257, C258, C261, C262).

[13] R. Hiptmair and J. Li. “Shape derivatives in differential forms I: an intrinsic perspective”. In: *Ann. Matematica Pura Appl.* 192 (2013), pp. 1077–1098. DOI: 10.1007/s10231-012-0259-9. (Cit. on p. C259).

[14] C. R. de Lima, L. A. Mello, R. G. Lima, and E. C. N. Silva. “Electrical impedance tomography through constrained sequential linear programming: a topology optimization approach”. In: *Meas. Sci. Tech.* 18.9 (2007), pp. 2847–2858. DOI: 10.1088/0957-0233/18/9/014. (Cit. on p. C257).

[15] M. Loeve. *Probability theory I*. Graduate Texts in Mathematics. Springer-Verlag, 1978. DOI: 10.1007/978-1-4684-9464-8. (Cit. on p. C259).

[16] R. Martin, S. Jonuscheit, A. Rio-Cristobal, and M. J. Doughty. “Repeatability of Pentacam peripheral corneal thickness measurements”. In: *Cont. Lens Anterior Eye* 38 (2015), pp. 424–429. DOI: 10.1016/j.clae.2015.05.001. (Cit. on p. C263).

[17] R. von Mises. “Mechanik der festen Körper im plastisch-deformablen Zustand”. In: *Nachrichten von der Gesellschaft der Wissenschaften zu Göttingen. Mathematisch-Physikalische Klasse* 1 (1913), pp. 562–592. URL: https://eudml.org/doc/58894 (cit. on p. C267).

[18] F. Orucoglu and E. Toker. “Comparative analysis of anterior segment parameters in normal and keratoconic eyes generated by Scheimpflug tomography”. In: *J. Ophthalmol.*, 925414 (2015), pp. 1–8. DOI: 10.1155/2015/925414. (Cit. on p. C263).

[19] D. C. Pye. “A clinical method for estimating the modulus of elasticity of the human cornea in vivo”. In: *PLOS One* 15 (2020), pp. 1–19. DOI: 10.1371/journal.pone.0224824. (Cit. on p. C263).

Author addresses

1. **M. Clarke**, School of Mathematics and Statistics, UNSW, Sydney, Australia.
   mailto:mike.a.clarke.93@gmail.com
2. **J. Dick**, School of Mathematics and Statistics, UNSW, Sydney, Australia.
   mailto:josef.dick@unsw.edu.au
3. **Q. T. Le Gia**, School of Mathematics and Statistics, UNSW, Sydney, Australia.
   mailto:qlegia@unsw.edu.au
4. **D. Pye**, School of Optometry and Vision Science, UNSW, Sydney, Australia.
   mailto:d.pye@unsw.edu.au